JOURNAL OF APPLIED PHYSICS **100**, 033908 (2006)

Particle size dependence of magnetization and phase transition near T_N in multiferroic $BiFeO_3$

R. Mazumder, S. Ghosh, P. Mondal, Dipten Bhattacharya,[a] S. Dasgupta, N. Das, and A. Sen
Sensor and Actuator Section, Central Glass and Ceramic Research Institute, Calcutta 700 032, India

A. K. Tyagi
Solid State and Surface Chemistry Section, Bhabha Atomic Research Center, Trombay, Mumbai 400 085, India

M. Sivakumar[b]
Ultrasonic Processing Group, National Institute of Advanced Industrial Science and Technology, Nagoya 463-8560, Japan

T. Takami and H. Ikuta
Department of Crystalline Materials Science, Nagoya University, Nagoya 464-8603, Japan

R. Mazumder, is presently with Nationa Institute of Technology Rourkela, ranabrata@nitrkl.ac.in

(Received 18 January 2006; accepted 15 June 2006; published online 14 August 2006)

We report results of a comprehensive study of the phase transition at T_N (~643 K) as a function of particle size in multiferroic $BiFeO_3$ system. We employed electrical, thermal, and temperature dependent x-ray diffraction studies in order to characterize the transition in a host of samples. We also carried out detailed magnetic measurements over a temperature regime of 2–300 K under a magnetic field of 100–10 000 Oe both on bulk and nanocrystalline systems. While in the bulk system a sharp endothermic peak at T_N together with a broad feature, ranging over nearly ~100 K (ΔT), could be observed in calorimetry, the nanoscale systems exhibit only the broad feature. The characteristic dielectric anomaly, expected at T_N, is found to occur both at T_O and T_N across ΔT in the bulk sample. The Maxwell-Wagner component due to interfaces between heterogenous regions with different conductivities is also present. The magnetic properties, measured at lower temperature, corroborate our observations in calorimetry. The metastability increases in the nanoscale $BiFeO_3$ with divergence between zero-field cooled and field cooled magnetizations below ~100 K and faster magnetic relaxation. Interestingly, in nanoscale $BiFeO_3$ one also observes finite coercivity at lower temperature, which points out that suitable design of particle size and shape may induce ferromagnetism. The inhomogeneous distribution of Bi/Fe ions and/or oxygen nonstoichiometry seems to be giving rise to broad features in thermal, magnetic as well as electrical responses. © *2006 American Institute of Physics*. [DOI: 10.1063/1.2229667]

I. INTRODUCTION

The multiferroics, with, at least, two of the three orders or degrees of freedom—(anti)ferromagnetic, (anti)ferroelectric, and ferroelastic—coexisting and often a coupling among them, are rare in nature as transition metal ions with active *d* electrons often tend to reduce the off-center distortion necessary for ferroelectricity.[1] It has been pointed out by a recent theoretical work[2] that additional electronic mechanism (mainly s^2 lone pair at another site) provides the driving force for ferroelectricity. Since the observation by Smolensky *et al.*[3] in 1958, three different classes of multiferroic systems could be identified—$R\mathrm{MnO_3}$ (where $R=\mathrm{Dy,Tb,Ho,Y,Lu}$, etc.), $R\mathrm{Mn_2O_5}$ (where $R=\mathrm{Nd,Sm,Dy,Tb}$), and $\mathrm{Bi}B\mathrm{O_3}$-type (where $B=\mathrm{Mn,Fe}$). Such systems depict magnetoelectric coupling and, therefore, magnetic polarization can be achieved by electric field and vice versa. Recently, there has been a renewed interest[4] in multiferroic systems due to the observation of orders of magnitude large magnetoelectric coupling and the application potential of these systems in a range of devices based on "spintronics," magnetoelectric sensors, electrically driven magnetic data storage and recording devices, magnetocapacitive devices, nonvolatile memories, etc. Direct evidence of linear coupling between electric and magnetic domains could be observed in $YMnO_3$ using nonlinear optics—optical second harmonic generation.[5] However, the temperature range over which the multiferroic behavior is observed varies from system to system. For instance, $R\mathrm{MnO_3}$ (space group $P6_3cm$) and $R\mathrm{Mn_2O_5}$ (space group *Pbam*) systems depict multiferroic properties at lower temperature (<100 K).[6] In $BiMnO_3$ (space group *C*2) too, ferromagnetic and ferroelectric orders coexist below ~105 K. The $BiFeO_3$ system (space group *R*3*c*) is interesting, in this respect, as it depicts ferroelectric order below $T_C \sim 1110$ K and antiferromagnetic order below $T_N \sim 643$ K. Therefore below T_N, one expects coupling between electric and magnetic domains.

The multiferroic nature of $BiFeO_3$ is due to stereochemical activity associated with the $6s^2$ lone pair of Bi^{3+}. It results in lowering of structural symmetry and hence

[a]Electronic mail: dipten@cgcri.res.in
[b]Present address: Bharathidasan University, Tamil Nadu, Tiruchirapalli 620024, India.

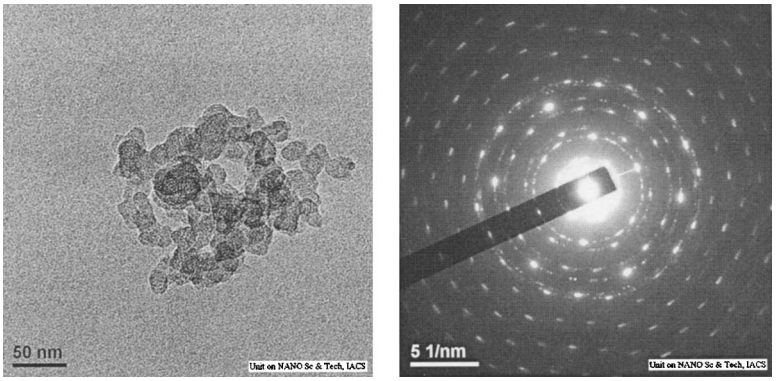

FIG. 1. Typical transmission electron microscopy (TEM) photograph of nanoscale $BiFeO_3$ system. The selected area electron diffraction (SAED) pattern is also shown. The nanoscale particles are crystalline in nature.

ferroelectricity.[7] The magnetic order is little complicated with ferromagnetic coupling within a plane and antiferromagnetic coupling between two adjacent planes. Due to antisymmetric Dzyaloshinsky-Moriya (DM) exchange interaction, canted antiferromagnetism may develop. However, a spiral spin structure is superimposed on this antiferromagnetic order in which the antiferromagnetic axis is rotated through the crystal and develops an incommensurate order.[8] The magnetoelectric coefficient (dE/dH) is found to vary within 3 V/cm Oe across a temperature range of 77–300 K.[9] The study of crystallographic structure using high temperature x-ray diffraction (XRD) patterns provides the ferroelectric Curie point (T_C) to be ~1110 K.[10] Direct measurement of polarization (P) versus electric field (E) loop or dielectric spectroscopy across T_C is still missing. The magnetic transition temperature (T_N) is estimated from magnetic structure study using neutron diffraction patterns and is found to be ~643 K.[11,12] Weak magnetization, however, restricts its large scale use in several devices. One needs to explore whether large magnetization can be induced in these systems by doping and/or structural manipulation. In other words, one needs a thermodynamically stable system with both ferromagnetism and ferroelectricity existing above room temperature. $BiFeO_3$ could not be exploited for any application for two major problems: (i) weak magnetization as it is essentially an antiferromagnet below T_N and (ii) large loss factor because of oxygen nonstoichiometry. Therefore, even though magnetoelectric coupling could be observed above room temperature, unlike $CdCr_2S_4$ (Ref. 13) complete ferroelectric polarization flop cannot be achieved in $BiFeO_3$ by magnetic field sweeping. It has recently been observed[14] that in thin film $BiFeO_3$, finite magnetization of the order of ~1 μ_B/Fe prevails even above room temperature. The origin of such magnetization is a bit controversial.[15] It has been proposed, however, that such finite magnetization could result from increased canting.[16] A suitable doping at Bi and/or Mn site, on the other hand, helps in minimizing the conductivity and hence the loss factor.[17] It will be interesting to explore whether both the problems can be addressed and tackled in nanoscale $BiFeO_3$.

In this paper, we report the results of a comprehensive study carried out both on bulk and nanoscale $BiFeO_3$ for exploring the phase transition features near T_N as well as the low temperature magnetic properties. We employed dc resistivity, dielectric measurements, differential scanning calorimetry (DSC), differential thermal analyses (DTAs), dilatometry, temperature dependent x-ray diffraction, and detailed magnetic measurements in order to systematically record the behaviors of the bulk and nanosystem below and above the magnetic transition point. It appears that the local inhomogeneity as well as oxygen nonstoichiometry across the sample volume have major roles to play in governing all the properties.

II. EXPERIMENTAL DETAILS

Primarily two types of measurements were carried out on phase pure bulk and nanoparticles of $BiFeO_3$—thermal and magnetic. The electrical measurements were carried out only on bulk-sintered samples. All the samples have been prepared by different solution chemistry routes. While bulk ~1 μm size particles have been prepared by conventional coprecipitation technique, finer 4–50 nm size particles have been prepared by sonochemical and solution evaporation (tartaric acid template or ferrioxalate precursor) techniques. In the sonochemical technique, powders are prepared in solution chemistry route under ultrasonic vibration. A mixed aqueous solution of $Bi(NO_3)_3$ and $Fe(NO_3)_2$—taken in proper stoichiometric ratio—is sonicated by using Ti horn (20 kHz, 1500 W, Vibracell, USA) until the precipitation is complete. A small amount of decalin is used for proper power transfer and sodium dodecyl sulphate (SDS) surfactant is also used for preventing agglomeration. The precipitated powder is collected, washed by alcohol, and dried in a vacuum oven at ~40 °C. In the tartaric acid template technique, aqueous solutions of metal nitrates were mixed with tartaric acid. The mixed solution was boiled at 150–160 °C until the liquid evaporated out. The green fluffy powder was heated for 1 h before calcination. The tartaric acid template helps in forming heterometallic polynuclear polymeric arrays where metal ions come in close proximity to yield phase pure $BiFeO_3$ after *in situ* oxidization. If oxalic acid is used as a template, it forms Bi-ferrioxalate precursor which undergoes decomposition in the presence of oxidizing agent such as HNO_3. In this case too, heteronuclear polymeric array, with metal ions, forms. Other organic acids such as citric acid do not give rise to such phase pure $BiFeO_3$ as it tends to form dimeric chain instead of polynuclear polymeric chain. It appears, therefore, that the formation of heteronuclear polymeric arrangement prior to oxidization is the key to the formation of phase pure $BiFeO_3$. The as-prepared powders were calcined at 400–700 °C and the bulk samples were

sintered at ~820 °C for 10 h. Both the bulk and nanoscale samples were characterized by XRD and scanning electron microscopy (SEM) studies. In addition, the nanoparticles have been studied by transmission electron microscopy (TEM). The specific surface area of the nanoparticles has also been measured. Further details of the sample preparation and the results of the characterization are available elsewhere.[18,19] The crystallite size of the nanoscale systems could be estimated from x-ray peak broadening by Debye-Scherrer equation using the full width at half maximum (FWHM) data. The particle sizes could be estimated from Brunauer-Emmett-Teller (BET) specific surface area data as well as directly from TEM photographs. A representative TEM photograph for nanoscale $BiFeO_3$ together with selected area electron diffraction pattern is shown in Fig. 1.

The thermal and magnetic measurements have been carried out on powder samples while electrical measurements have been carried out on sintered pellets. The DSC study has been carried out in Perkin-Elmer Diamond DSC over a temperature range of 300–800 K while the DTA measurements were carried out in Shimadzu DTA-50. The heating rate was 10 °C/min in all the cases. The thermal expansion has been measured in Orton dilatometer (model 1600). The low-frequency (10 Hz–1 MHz) dielectric measurements have been carried out in an *LCR* meter (Hioki hi-tester 3652-50). The electrodes have been prepared by silver coating and the coating was cured at ~600 °C in air.

The magnetic measurements have been carried out in a superconducting quantum interference device (SQUID) magnetometer [magnetic property measurement system (MPMS)] of Quantum Design. The zero-field cooled (ZFC) and field cooled (FC) magnetization versus temperature patterns have been studied across a temperature range of 2–300 K while magnetic hysteresis loops over ±10 000 Oe have been recorded at several temperatures. We also carried out magnetic relaxation measurements at ~5 and ~300 K under ~100 and ~10 000 Oe for both bulk and nanoscale samples.

III. RESULTS AND DISCUSSION

A. Thermal studies

In Fig. 2(a), we show the specific heat (C_p) vs temperature patterns—extracted from DSC and DTA data—for both bulk and nanoscale $BiFeO_3$. The specific heat is found to be increasing as a function of particle size. This could be because of decrease in surface area to volume ratio and consequent local structural rearrangement with the increase in particle size. A small yet sharp peak—signifying first order transition—could be noticed at ~653 K (T_N) in the case of bulk sample. In the inset of Fig. 2(a), we show the (C_p/T) versus temperature (T) plot of the region around the peak for the bulk sample. The change in entropy ΔS [$=\int(C_p/T)dT$] is estimated to be ~0.0612 J/g K. In Fig. 2(b), we show the thermal expansion data for the bulk sample. The phase transition feature is clearly evident near T_N.

Apart from the rise in specific heat with the increase in particle size, one can also notice a variation in the phase transition feature with the particle size. For finer particles, a very broad feature—spanning nearly 200 K—appears while with the increase in particle size (≥50 nm), the broadness reduces a bit, and the feature near T_N becomes more prominent. The absence of a sharp peak clearly points out local inhomogeneity and broad phase transition across a wide temperature range. Although, such broad feature could be observed in bulk samples as well, simultaneous presence of sharp peak highlights more ordering in bulk sample. It is to be noted in this context that no structural phase transition is noticed across T_N in $BiFeO_3$.[20] Our high temperature XRD study too does not depict any structural transition at T_N. The magnetic phase transition at T_N, of course, is associated with colossal phonon anomaly as well as anomaly in dielectric

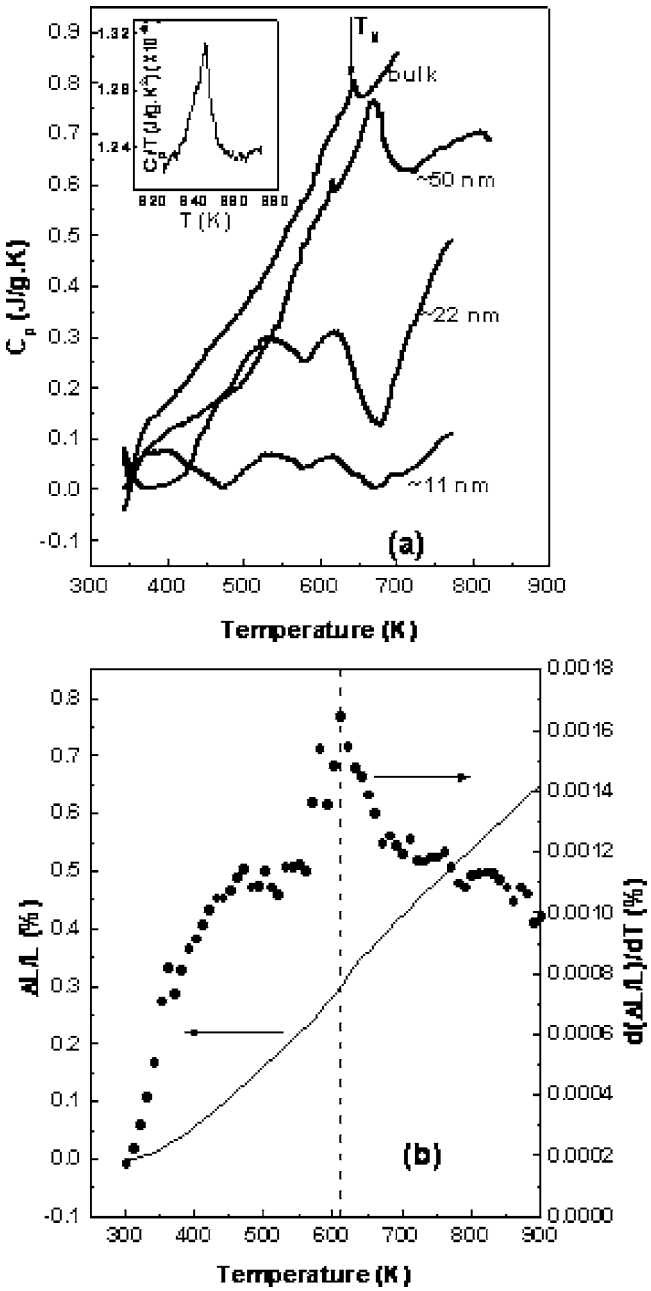

FIG. 2. (a) The specific heat (C_p) vs temperature (T) plots for the bulk and nanoscale $BiFeO_3$; inset: C_p/T vs temperature for the bulk sample around T_N; (b) the thermal expansion vs temperature plot for the bulk $BiFeO_3$ sample. The variation of thermal expansion coefficient (α) with temperature is also shown.

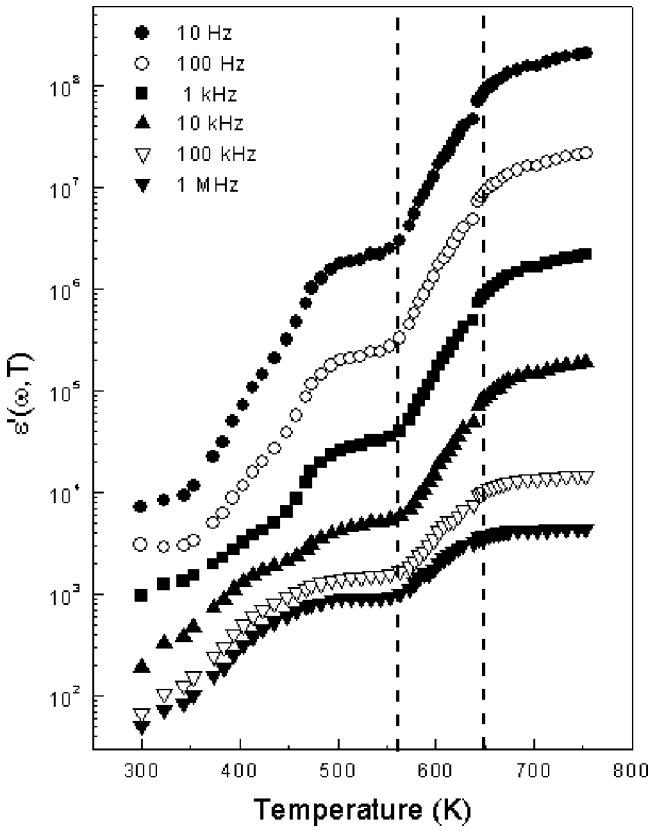

FIG. 3. The real part of the dielectric permittivity vs temperature for the bulk $BiFeO_3$ sample. It appears that there are two dielectric anomalies across a temperature range $\Delta T \sim 100$ K.

response due to magnetoelectric effect. Finite latent heat and change in thermal expansion coefficient as observed in this work could be due to strong spin-phonon coupling.

The nanocrystalline samples contain primarily inhomogeneous phases where lattice defects, oxygen nonstoichiometry, etc., appear to be sizable. In addition, lattice strain is also high in nanocrystalline system. The combined effect has given rise to even smaller scale of homogeneity in nanosystem. Such inhomogeneity together with increased surface to volume ratio in nanosized particles could give rise to suppression of antiferromagnetic order especially for 11 nm particles. As a result, at least in global calorimetry, no clear endothermic peak could be observed. In the absence of a sharp peak in nanocrystalline samples, it is difficult to identify the phase transition temperature and its shift as a function of particle size. Of course, for a particle size range of 20–50 nm, Chattopadhyay *et al.*[21] have observed decrease in T_N down to ~603 K.

B. Electrical studies

In Fig. 3, we show the real part of the dielectric permittivity versus temperature for the bulk sample across a temperature range of 300–673 K. The impedance (Z) and the dielectric loss spectra at different temperatures are shown in Figs. 4 and 5. We show here the data corresponding to the frequency range of 100 Hz–1 MHz. The real dielectric permittivity $[\varepsilon'(\omega,T)]$ exhibits two anomalies—at T_O and T_N—over a temperature span ~100 K (ΔT) (Fig. 3). In order

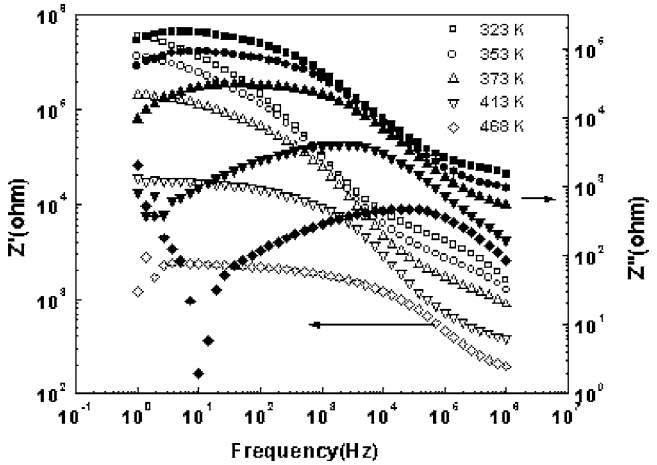

FIG. 4. The real and imaginary impedances vs frequency plot at several temperatures for the bulk $BiFeO_3$.

to figure out whether the anomalies in dielectric permittivity originate from intrinsic features or not, we carried out equivalent circuit analysis of the impedance spectra.[22] Typical complex-plane impedance spectra are shown in Fig. 6. The circuit analysis shows that it is possible to separate the grain and grain boundary or interface contribution to the overall impedance spectra. The equivalent circuit is shown in the inset of Fig. 6—series combination of parallel resistance (R) and capacitance (C) paths. Such separation helps in extracting the intrinsic capacitance of the system. The plot of intrinsic capacitance versus temperature is shown in Fig. 7. It is clear that the pattern is almost similar to what has been observed in Fig. 3. The dielectric anomalies near T_O and T_N are conspicuous. Therefore, the dielectric anomalies are intrinsic and could not be due to extrinsic factors such as electrode-sample interface or other interfaces such as grain boundaries. The temperature T_O marks the onset (~550 K) and T_N marks the termination of the transition process. One expects anomaly in dielectric permittivity due to strong magnetoelectric coupling. Two anomalies across ΔT—instead of only one at T_N—result from broadening of the magnetic transition due to inhomogeneity. The dielectric permittivity exhibits high value and large frequency dispersion both below and above the phase transition range ΔT. Therefore from all

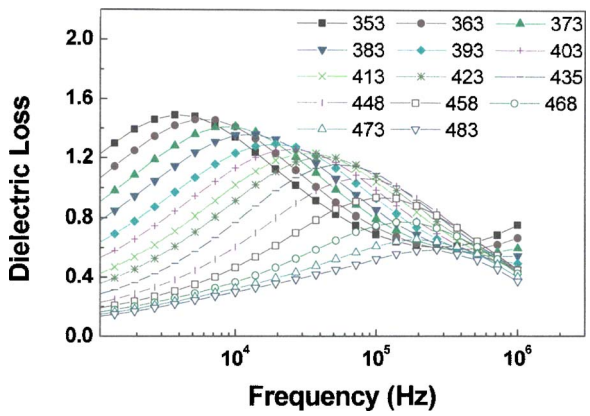

FIG. 5. (Color online) The dielectric loss spectra at different temperatures for the bulk $BiFeO_3$.

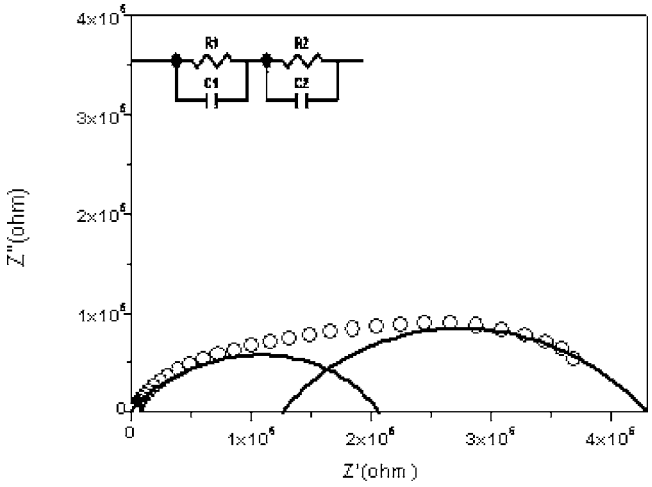

FIG. 6. A typical impedance spectrum in complex-plane impedance plot. The solid lines signify the fitting. The equivalent circuit is shown in the inset.

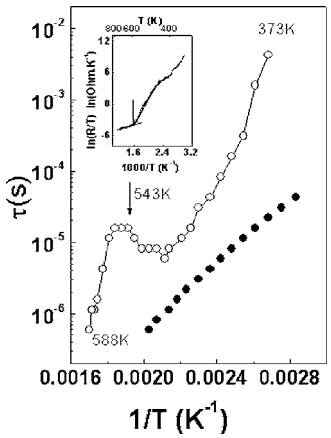

FIG. 8. The dielectric relaxation time vs inverse temperature plot. While the open symbols signify the relaxation time (τ_Z) estimated from impedance spectra, the solid symbols signify the relaxation time (τ_ε) estimated from dielectric loss spectra. In the inset, the $\ln(R_{dc}/T)$ vs inverse temperature plot is shown where R_{dc} is four-probe dc resistance of the bulk $BiFeO_3$.

these data and analyses, it can be established that inhomogeneity, even in the bulk $BiFeO_3$ sample, leads to broadening of the transition at T_N.

We now turn to the dielectric relaxation process and estimation of relaxation time in bulk $BiFeO_3$. It has been observed in the impedance or dielectric loss spectra that the relaxation process here is essentially non-Debye; the full width at half maximum for the relaxation peaks is always higher than 1.144 decade, which is expected in Debye relaxation model. In such a relaxation process, one expects a spectrum of relaxation times with three prominent modes τ_Z, τ_ε, and τ_M, where τ_Z, τ_ε, and τ_M are the average relaxation times estimated from impedance, dielectric, and modulus spectra, respectively.[23,24] It is generally observed that $\tau_Z \leqslant \tau_\varepsilon \leqslant \tau_M$. The elements such as resistance (R) and capacitance (C) become inherently frequency dependent.[25] The exponent of the frequency dependence of these parameters can be extracted from the analysis of depression of the center of semicircle below the abscissa in complex-plane impedance spectra plot (Fig. 6). The estimated frequency dependence of R and C helps in collapsing the relaxation peaks in impedance, dielectric, and modulus spectra onto a single peak frequency. Of course, in the case of Debye relaxation with dielectric relaxation strength $\Delta\varepsilon=0$, one observes convergence of these three relaxation time scales. Rigorous derivation of τ_Z, τ_ε, and τ_M and their correlation under different conditions—Debye and non-Debye—are available in Ref. 24. Detailed study on correlation among inhomogeneity, wider transition range (ΔT), and dielectric relaxation process for a series of bulk $BiFeO_3$ will be reported elsewhere. For the present case, we have analyzed the impedance as well as dielectric loss spectra in order to figure out the relaxation time scales. The intrinsic relaxation time scales τ_Z and τ_ε are plotted as a function of temperature (T) in Fig. 8. Since τ_ε becomes smaller than the frequency window used in this work beyond ~473 K, we could not estimate τ_ε across T_N. A broad anomaly quite akin to that observed in the case of $\varepsilon'(\omega,T)$ vs T (Fig. 3), however, is observed in the case of τ_Z vs T pattern. Below the anomaly at T_O, the τ_Z vs T pattern turns out be nearly Arrhenius while above the anomaly too, the pattern appears to be Arrhenius. In the inset of Fig. 8 we show the natural log of four-probe dc resistivity vs $1/T$ pattern. The activation energies from both τ_Z-$1/T$ and resistivity vs $1/T$ patterns have been calculated. While the activation energies, calculated from resistivity data, turn out to be ~0.88 and 0.19 eV at below T_O and above, they are 0.46 and 0.9 eV over the same temperature ranges when estimated from relaxation time scale vs temperature data. The difference in the values of the activation energies, calculated from resistivity and relaxation time data, signifies that the mechanism of relaxation of the electric polarization is different from simple polaron hopping. Dielectric relaxation is taking place through a complicated and correlated process of local structural rearrangement along with hopping of charge carriers.

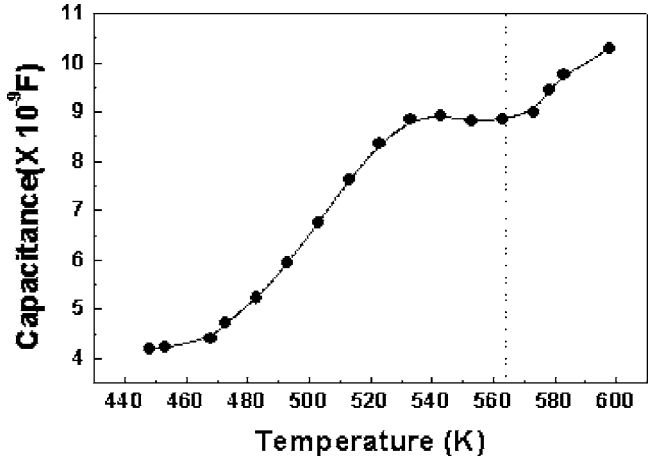

FIG. 7. The intrinsic capacitance, as estimated from equivalent circuit analysis, vs temperature plot. The similarity between this plot and the plots in Fig. 3 is conspicuous.

Therefore, the overall dielectric response appears to be consisting of both interface and intrinsic polarization components. Clear dielectric anomaly could be observed near T_N due to magnetoelectric effect in $BiFeO_3$. However, the transition region becomes broad, spanning over a temperature range ΔT, due to inhomogeneity and/or oxygen nonstoichi-

ometry. Because of such inhomogeneity, a spectrum of relaxation times with $\tau_Z < \tau_\varepsilon$ could be noticed in the present case. The inhomogeneity results from volatility of Bi near the processing temperature of 820–850 °C and/or oxygen nonstoichiometry inherent in the complicated crystal chemistry of $BiFeO_3$. In fact, the polarization (P) vs field (E) loop in the case of pure $BiFeO_3$ appears to reflect the lossy nature. The inhomogeneity results in smaller ferroelectric domains with faster relaxation dynamics. It would have been interesting to study the relaxation dynamics and transition point in nanoscale system where the scale of inhomogeneity is higher and the homogeneous cluster size is small. Since sintering leads to growth of nanograins into micron size, no electrical measurement could be done on nanocrystalline samples.

C. Magnetic studies

We have measured ZFC and FC magnetizations versus temperature patterns under different fields as well as hysteresis loops at several temperatures across a range of 2–300 K. The magnetic relaxation pattern has also been observed at different temperatures and under different fields. In Fig. 9, we show the ZFC and FC magnetizations versus temperature patterns for both the bulk and nanocrystalline $BiFeO_3$. The bulk system exhibits antiferromagnetic order below $T_N \sim 643$ K. Therefore, we could not study the magnetization across the transition point. The magnetization at ~2 K is found to be $\sim 0.016\mu_B$/Fe atom under ~100 Oe and $\sim 1.5\mu_B$/Fe atom under ~10 000 Oe for the bulk sample. It drops down to $\sim 0.008\mu_B$/Fe atom and $0.7\mu_B$/Fe atom, respectively at ~300 K. On the other hand, for nanoscale sample, the low temperature magnetization (at ~2 K) is found to be nearly equal to what has been observed in the case of bulk sample. But, at ~300 K, the magnetization is higher by a factor of 2. For high spin ($S=5/2$) Fe^{3+} ions, the effective magnetization should be $\sim 5.92\mu_B$. Therefore, it appears that the spin configuration per Fe ion is far from parallel. There are several other important points worthy of noting in the magnetization versus temperature data: (i) no divergence between ZFC and FC data in the case of the bulk sample; (ii) the magnetization changes with magnetic field; (iii) in the case of nanoscale sample, the ZFC and FC magnetization data diverge below ~100 K; (iv) in all the cases—bulk and nano—the magnetization rises with decrease in temperature; (v) the temperature below which the magnetization starts rising is ~50 K for the bulk sample and ~10 K for the nanoscale sample. The sharp rise in magnetization below ~50 K, in bulk sample, could result from free Fe ions. In the absence of high temperature magnetization data above T_N, this Curie-Weiss paramagnetism due to free Fe ions could not be quantitatively estimated. Interestingly, in the case of bulk sample an anomaly near ~65 K could be observed in the low-field ZFC data. The FC as well as high-field data, of course, do not depict any such anomaly. This seems to be because of an impurity phase $Bi_2Fe_4O_9$. Of course, such a phase could not be detected in x-ray diffraction pattern. The absence of the peak in FC data signifies metastability of that phase under field. The nanoparticles of the $BiFeO_3$ do not depict any anomaly around ~65 K.

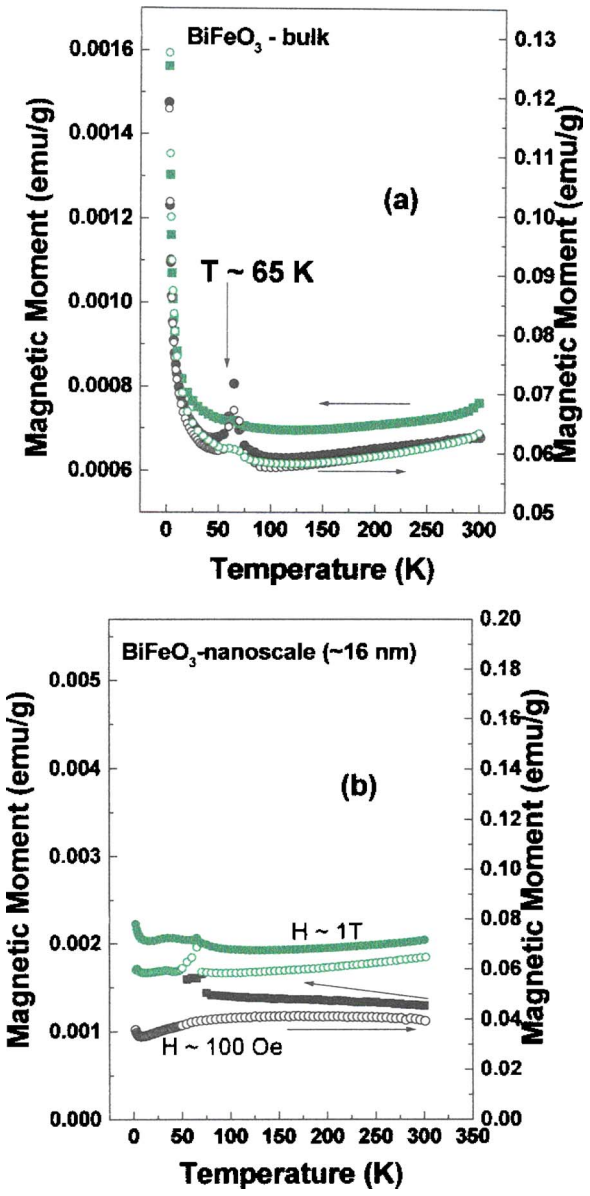

FIG. 9. (Color online) The zero-field cooled and field cooled magnetization vs temperature plots for the (a) bulk and (b) nanoscale $BiFeO_3$ under the applied fields—100 and 10 000 Oe. The green colored plots are data for ~10 000 Oe. The open symbols denote the zero-field cooled data while the solid symbols denote the field cooled data.

Because of stable antiferromagnetic order within the temperature range of 2–300 K, no divergence between ZFC and FC magnetization versus temperature plots could be noticed in the case of bulk sample. The nanoscale sample, on the other hand, exhibits divergence between ZFC and FC magnetization data below ~100 K, which could be due to the onset of spin glass state. The magnetization at any temperature, within this regime, depends on history effect—the path followed for reaching the point. The ZFC data exhibit a broad cusplike feature below ~100 K which is typical of nanoscale antiferromagnetic system.[26]

In Figs. 10 and 11 we show the hysteresis loops for bulk and nanoparticle systems. For the bulk $BiFeO_3$ sample, the hysteresis loops at several temperatures exhibit patterns typical of an antiferromagnetic system with no hysteresis and nearly zero coercivity. Small diamagnetic component ob-

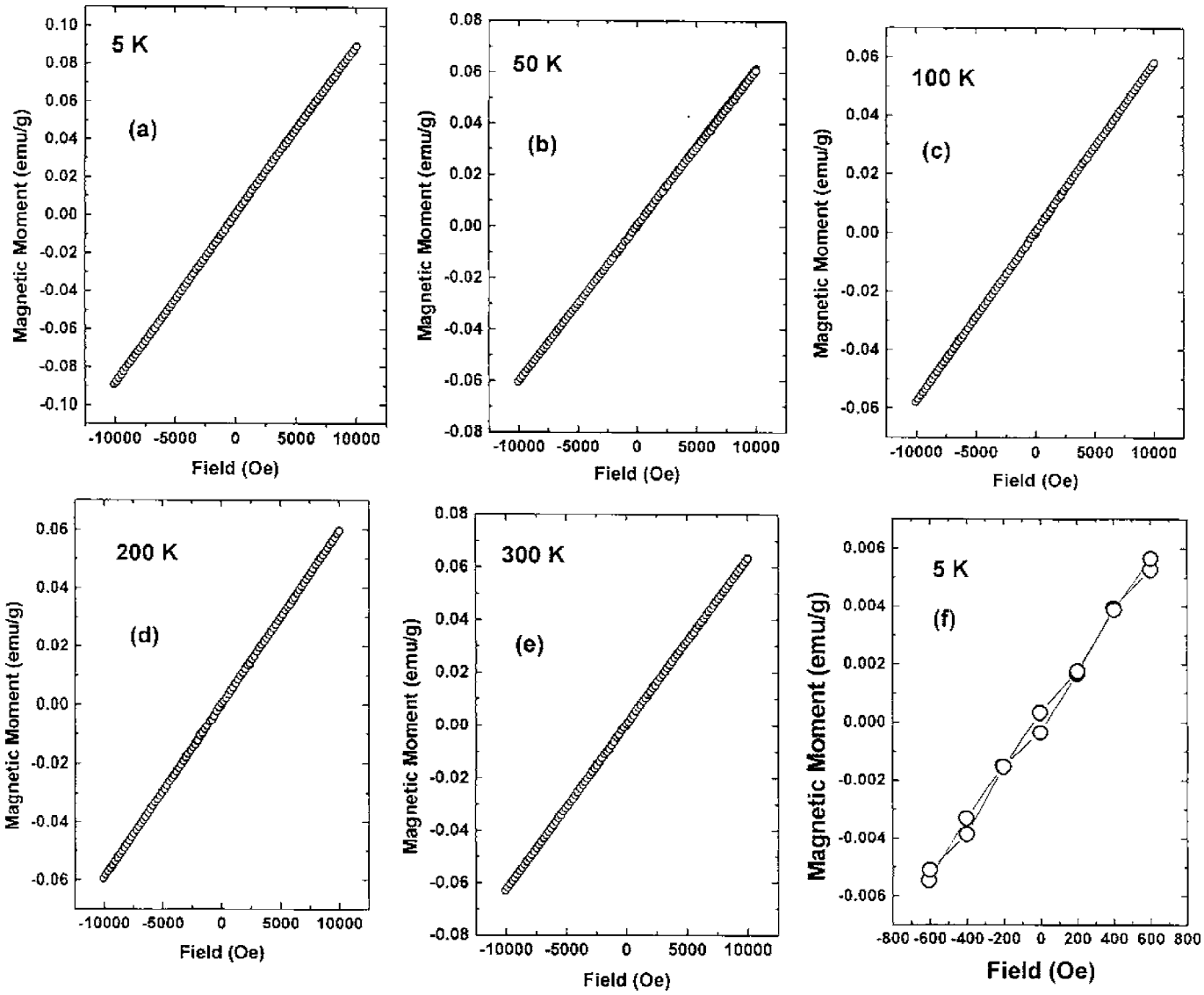

FIG. 10. [(a)–(e)] The magnetic hysteresis loops at different temperatures for the bulk $BiFeO_3$ sample. (f) The low-field portion of the hysteresis loop at 5 K is blown up.

served in the hysteresis data at very low field is due to the contribution from the sample holder. It becomes prominent in the case of antiferromagnetic sample with very small magnetic moment. The nanoparticle system, on the other hand, exhibits sizable hysteresis and finite coercivity below ~100 K. In fact, one can easily notice a deviation from linearity and formation of a ferromagnetic loop at a lower field. The coercivity at ~5 K is found to be ~450 Oe. An observation of such high coercivity in nanoscale $BiFeO_3$ is quite significant. This could be because of lattice strain-induced spin canting or ferromagnetism in nanoscale. It has been reported earlier that lattice strain in thin film gives rise to higher magnetism ($\sim 1\mu_B$/Fe). The observation of higher coercivity in nanoscale may help in finding a way for improving magnetization in $BiFeO_3$, which, in turn, will lead to many applications.

In order to find out the stability of the magnetic phases—both at low temperature (~5 K) and room temperature (~300 K)—in the nanoparticle vis-à-vis bulk system, we measured the magnetic relaxation pattern over a time scale of ~36 000 s. The relaxation patterns are shown in Fig. 12. In all the cases of the relaxation measurements, the zero-field cooling protocol has been used. The temperature of the sample is set at the desired point under zero magnetic field. Once the temperature is reached, the field is applied and the relaxation of the magnetic moment is measured over a time scale of ~36 000 s without switching off the applied field. The amount of variation in initial magnetization (M_0) with time (t) varies with temperature, applied field, and sample type—bulk or nanoparticle systems. The initial magnetization decreases with time in the case of low field (~100 Oe) while it increases with time in the case of higher field (~10 000 Oe). In all the cases, however, the pattern of variation is logarithmic in nature where the magnetization at any time t follows $M(t,T)=M_0(T)\pm S(T)\ln(t/\tau_m)$ equation; S is magnetic viscosity and is related to the activation energy, and τ_m is a characteristic time scale. This is a typical flux-creep pattern. The extent of relaxation in the bulk system is negligible at low temperature and is very small (~0.53%) at

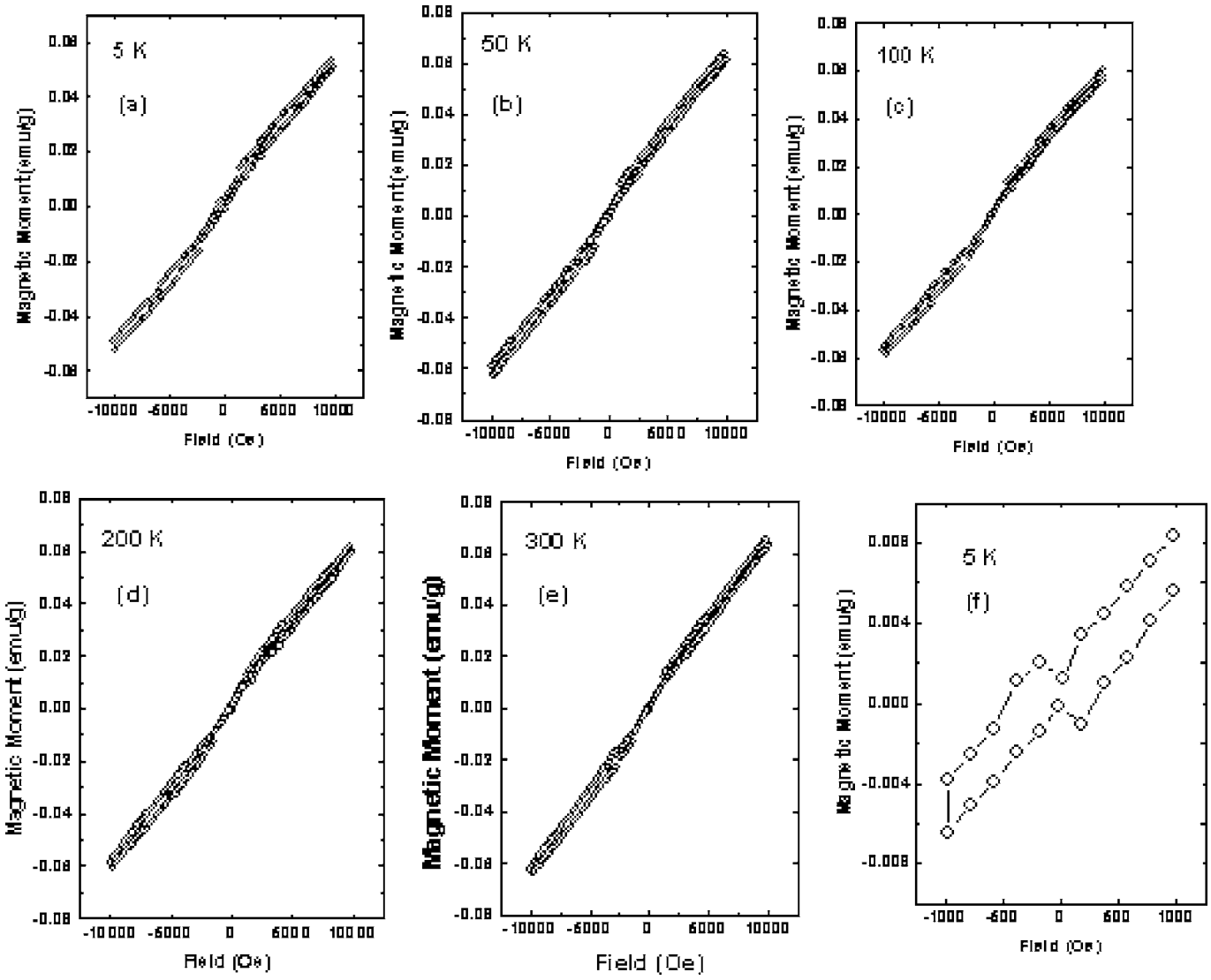

FIG. 11. [(a)–(e)] The magnetic hysteresis loops at different temperatures for the nanoscale $BiFeO_3$ sample. (f) The low-field portion of the hysteresis loop at 5 K is blown up.

high temperature highlighting the stability of the phase. The nanoparticle system, of course, exhibits large relaxation ($\sim$0.61%) at low temperature and nearly an order of magnitude higher relaxation ($\sim$3.7%) than that of the bulk system at high temperature. The high-field relaxation patterns depict a rise in magnetization. This could be due to metastability in the system. The activation energies are found to be varying over $\sim$0.08–0.25 eV with field (100–10 000 Oe) at $\sim$5 K and over 1.4–10.0 eV at $\sim$300 K. In bulk sample, of course, the variation in the magnetization is very small both at $\sim$5 and $\sim$300 K. The activation energies for the bulk systems are found to be enormous—of the order of $\sim 10^4$ eV—reflecting the stability of the magnetic phases.

These results point out that a magnetic state with a higher magnetization and a finite coercivity develop in the case of nanoscale samples. Of course, the magnetic state is metastable with lower activation energy and higher relaxation rate. The metastability is possibly due to spin frustration in nanoscale.

IV. SUMMARY

In summary, we have studied the phase transition near T_N as a function of particle size in multiferroic $BiFeO_3$ system by employing calorimetry, dielectric, and temperature dependent x-ray diffraction studies. Because of inhomogeneity, the phase transition at T_N is found to become broader—both in bulk and in nanoscale samples. The inhomogeneity possibly arises from volatility of Bi near the processing temperature as well as susceptibility of the lattice structure for developing oxygen nonstoichiometry. Such broader transition gives rise to two anomalies in dielectric permittivity across a range ΔT in the case of bulk sample. The magnetization versus temperature data depict a rise in magnetization at lower temperature for both the cases while an onset of spin glass state in the case of nanoscale sample below $\sim$100 K. The magnetization in the latter case relaxes at a faster rate and yields lower activation energy. One interesting observation is the ferromagnetism and finite coercivity at lower temperature ($<$100 K) in nanoscale, which possibly results from

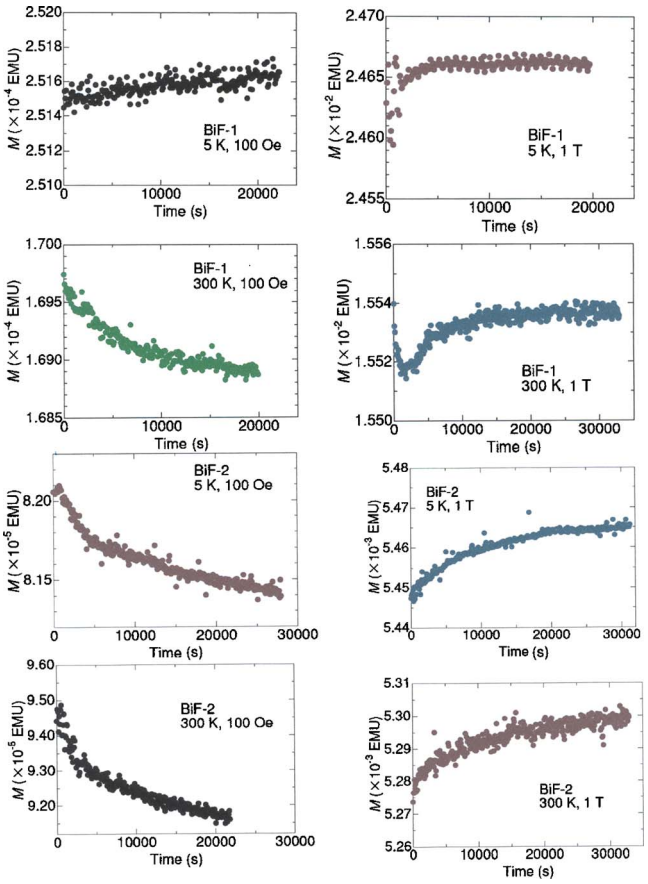

FIG. 12. (Color online) The magnetic relaxation patterns for the bulk and nanoscale $BiFeO_3$ under different fields and at different temperatures. BiF-1 and BiF-2 correspond to bulk and nanoscale samples, respectively.

enhanced lattice strain. This result points out that suitable design of $BiFeO_3$ particles—size and shape—can improve the magnetization of the system.

ACKNOWLEDGMENT

This work has been carried out under the network program "Custom-Tailored Special Materials" (CMM 0022) of CSIR, Government of India. One of the authors (R.M.) thanks CSIR for a senior research fellowship.

[1] H. Schmid, Ferroelectrics **162**, 317 (1994).
[2] N. A. Hill, J. Phys. Chem. B **104**, 6694 (2000).
[3] G. A. Smolensky, A. I. Agranovskaya, and V. A. Isupov, Sov. Phys. Solid State **1**, 149 (1959).
[4] See, for example, M. Fiebig, J. Phys. D **38**, R123 (2005).
[5] M. Fiebig, Th. Lottermoser, D. Froelich, A. V. Goltsev, and R. V. Pisarev, Nature (London) **419**, 818 (2002).
[6] T. Kimura, T. Goto, H. Shintani, K. Ishizaka, T. Arima, and Y. Tokura, Nature (London) **426**, 55 (2003); T. Lottermoser, T. Lonkai, U. Amann, D. Hohlwein, J. Ihringer, and M. Fiebig, *ibid.* **430**, 541 (2004).
[7] P. Baettig, C. Ederer, and N. A. Spaldin, Phys. Rev. B **72**, 214105 (2005).
[8] I. Sosnowska, T. Peterlin-Neumaier, and E. Streichele, J. Phys. C **15**, 4835 (1982); C. Ederer and N. A. Spaldin, Phys. Rev. B **71**, 060401(R) (2005).
[9] M. Mahesh Kumar, A. Srinivas, S. V. Suryanarayana, G. S. Kumar, and T. Bhimasankaram, Bull. Mater. Sci. **21**, 251 (1998).
[10] J. D. Bucci, B. K. Robertson, and W. J. James, J. Appl. Crystallogr. **5**, 187 (1972).
[11] I. Sosnowska, T. Paterlin-Neumaier, and E. Steichele, J. Phys. C **15**, 4835 (1982).
[12] C. Blaauw and F. van der Woude, J. Phys. C **6**, 1422 (1973).
[13] J. Hemberger, P. Lukenheimer, R. Fichtl, H.-A. Krug von Nidda, V. Tsurkan, and A. Loidl, Nature (London) **434**, 364 (2005).
[14] J. Wang *et al.*, Science **299**, 1719 (2003).
[15] W. Eerenstein, F. D. Morrison, J. Dhu, M. G. Blamire, J. F. Scott, and N. D. Mathur, Science **307**, 1203a (2005).
[16] J. Wang *et al.*, Science **307**, 1203b (2005).
[17] X. Qi, J. Dho, R. Tomov, M. G. Blamire, and J. L. Macmanus-Driscoll, Appl. Phys. Lett. **86**, 062903 (2005); Y.-K. Jun, W.-T. Moon, C.-M. Chang, H.-S. Kim, H. S. Ryu, J. W. Kim, K. H. Kim, and S.-H. Hong, Solid State Commun. **135**, 133 (2005); V. R. Palkar, D. C. Kundaliya, and S. K. Malik, J. Appl. Phys. **93**, 4337 (2003).
[18] S. Ghosh S. Dasgupta, A. Sen, and H. S. Maiti, J. Am. Ceram. Soc. **88**, 1349 (2005).
[19] S. Ghosh, S. Dasgupta, A. Sen, and H. S. Maiti, Mater. Res. Bull. **40**, 2073 (2005).
[20] S. V. Kiselev, R. P. Ozerov, and G. S. Zhdanov, Sov. Phys. Dokl. **7**, 742 (1963).
[21] S. Chattopadhyay, S. D. Kelly, V. R. Palkar, L. Fan, and C. U. Segre, Phys. Scr., T **T115**, 709 (2005).
[22] P. Lukenheimer, R. Fichtl, S. G. Ebbinghaus, and A. Loidl, Phys. Rev. B **70**, 172102 (2004).
[23] See, for example, A. K. Jonscher, Nature (London) **267**, 673 (1977).
[24] J. F. Cordaro and M. Tomozawa, J. Am. Ceram. Soc. **64**, 713 (1981) and all the relevant references therein.
[25] See, for example, P. Victor, S. Bhattacharyya, and S. B. Krupanidhi, J. Appl. Phys. **94**, 5135 (2003) and all the relevant references therein.
[26] T. G. Sorop, M. Evangelisti, M. Haase, and L. J. de Jongh, J. Magn. Magn. Mater. **272–276**, 1573 (2004).